Short Communications

J. Synchrotron Rad. (2000). **7**, 280–282

Phase-contrast X-ray imaging with a large monolithic X-ray interferometer

Tohoru Takeda,[a]* Atsushi Momose,[b] Quanwen Yu,[a] Jin Wu,[a] Keiichi Hirano[c] and Yuji Itai[a]

[a]Department of Radiology, Institute of Clinical Medicine, University of Tsukuba, 1-1-1 Tennodai, Tsukuba-shi, Ibaraki 305-8575, Japan, [b]Advanced Research Laboratory, Hitachi Ltd, Hatoyama, Saitama 350-0395, Japan, and [c]Institute of Materials Structure Science, High Energy Accelerator Research Organization, Tsukuba-shi, Ibaraki 305-0801, Japan. E-mail: ttakeda@md.tsukuba.ac.jp

(*Received 2 February 2000; accepted 16 March 2000*)

To increase the field of view for large objects in phase-contrast X-ray imaging, a large monolithic X-ray interferometer has been fabricated using an available silicon ingot of diameter 10 cm. A performance study of this interferometer has been carried out using a synchrotron X-ray source. The view size of the interference pattern obtained with this interferometer was 25 mm wide and 15 mm high and its visibility was 79%. Various structures of a sliced human hepatocellular carcinoma were identified as necrosis, hemorrhagic necrosis, normal liver tissue and blood vessel. The performance of this interferometer was sufficient for phase-contrast X-ray imaging.

Keywords: phase-contrast X-ray imaging; monolithic X-ray interferometer; diagnostic radiology; cancer.

1. Introduction

Phase-contrast X-ray imaging using an X-ray interferometer (Bonse & Hart, 1965) has great potential for revealing the structures inside soft tissues without using a contrast agent because a sensitivity of ~1000 times higher is obtained using this method compared with the conventional method, which depends on the differences in X-ray absorption (Momose & Fukuda, 1995; Takeda *et al.*, 1995). A slice of a rat cerebellum (Momose & Fukuda, 1995) and a human metastatic liver tumor (Takeda *et al.*, 1995) were imaged and the various structures could be revealed. Phase-contrast X-ray computed tomography (Momose, 1995) has demonstrated rabbit cancer lesions (Momose *et al.*, 1996*a*,*b*), rat brain (Beckmann *et al.*, 1997, 1999) and human cancer lesions (Momose, Takeda, Itai & Hirano, 1998; Momose *et al.*, 1999; Takeda *et al.*, 1998; Takeda, Momose, Yu *et al.*, 2000; Takeda, Momose, Hirano *et al.*, 2000).

However, the available view size has been limited to 5 mm × 5 mm in the previous phase-contrast X-ray imaging system (Momose, Takeda, Itai, Yoneyama & Hirano, 1998) because of the small size of the monolithic X-ray interferometer. To obtain phase-contrast X-ray images of larger samples, a larger monolithic X-ray interferometer having a field of view of 25 mm × 25 mm has been constructed using a commercially available silicon ingot of diameter 10 cm. A performance study of this large monolithic X-ray interferometer was carried out using a synchrotron X-ray source, and the first experimental results are described in this paper.

2. Methods and material

2.1. *Large monolithic X-ray interferometer*

In a Laue-case monolithic X-ray interferometer, a field of view of 25 mm × 25 mm is expected by the geometrical beam path for 17.7 keV X-rays with Si 220 diffraction. The large monolithic X-ray interferometer [Si(220)] was cut (Sharan Ltd, Japan) from a highly perfect single-crystal silicon ingot of diameter 10 cm (Shintetsu-kagaku Ltd, Japan), providing four parallel X-ray half mirrors [a beam splitter (S), two mirrors (M1, M2) and an analyser (A)] in a skew symmetric alignment (Fig. 1). The spacings between S and M1, and M1 and A were 110 mm and 150 mm, respectively, within an error of 30 μm, to prevent degradation of the spatial coherency. The thickness of the half mirror was 1.0 mm. The width and height of S and A were 75 mm and 35 mm, respectively.

2.2. *Object*

A slice of a pathological specimen of human hepatocellular carcinoma (HCC) without cirrhosis, fixed in formalin, was placed in a cell filled with water. The cell was inserted into the beam path between M1 and A of the interferometer. The size of the slice was 25 mm × 25 mm with a thickness of 2 mm.

2.3. *Experimental procedure*

The experiment was performed at the three-pole superconducting vertical wiggler beamline BL-14B of the Photon Factory in Tsukuba, Japan. The experimental set-up is shown in Fig. 1(*a*). The X-ray energy was set at 17.7 keV by the monochromator installed upstream (not shown), and the beam was expanded with an Si(220) asymmetric-cut crystal and introduced into the interferometer. The X-ray flux in front of the sample was estimated to be $\sim 2 \times 10^6$ photons mm^{-2} s^{-1}. The typical beam current of the storage ring was 350 mA with an energy of 2.5 GeV.

To evaluate the fringe visibility, an interference pattern was recorded on an imaging plate (BAS-SR, IP-2025, Fuji Co. Ltd) with an exposure of 2 s. The imaging plate was processed by an image reader (BAS 5000, Fuji Co. Ltd) at a spatial resolution of 0.025 mm with 16 bit resolution.

The spatial distribution of the phase shift caused by a sample (phase map) can be obtained from several interference patterns using the technique of phase-shifting interferometry (Momose & Fukuda, 1995). As the interference patterns must be processed by computer, we used an X-ray sensing pick-up tube which acquired images on-line with a pixel size of 12 μm (horizontal) × 18 μm (vertical). An interference pattern was acquired with an exposure of 3 s. The phase map of the sample was obtained from five interference patterns that were measured sequentially by changing the phase of the reference beam. As the view size of the X-ray pick-up tube was 9.2 mm × 13.8 mm, the phase map of a pathological specimen was produced by combining four phase-maps of different areas.

3. Results and discussion

Fig. 2 shows an X-ray interference pattern obtained using the large monolithic X-ray interferometer with an exposure of 2 s. The

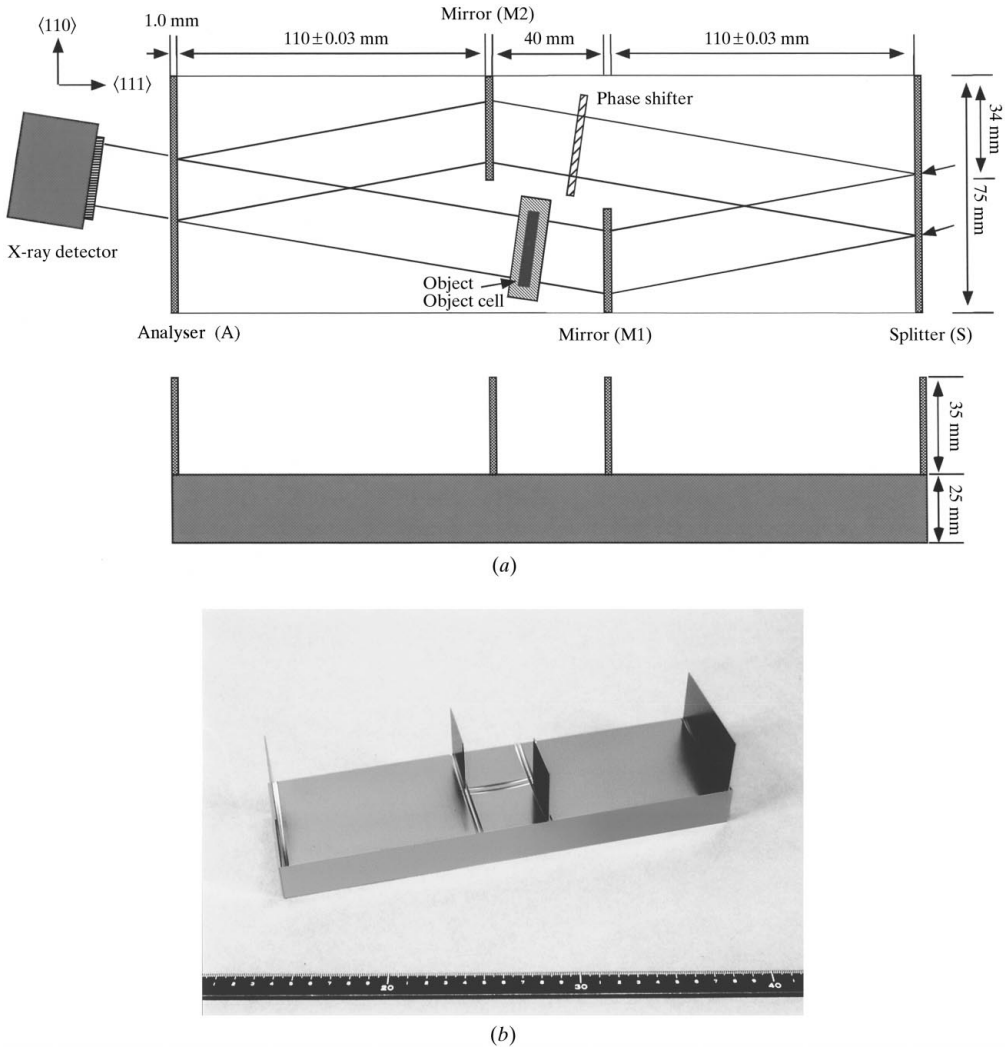

Figure 1
(*a*) Experimental set-up and schematic drawing of the large X-ray interferometer. (*b*) Photograph of the large X-ray interferometer.

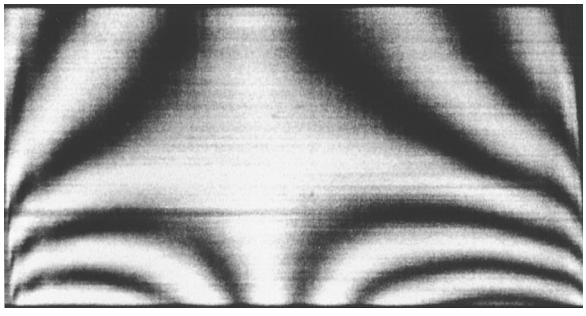

Figure 2
Interference pattern obtained using the large X-ray interferometer recorded using an imaging plate.

width and height of the interference pattern is 25 mm and 15 mm, respectively. Although the interferometer was designed and fabricated to produce 25 mm × 25 mm interference patterns, the height (15 mm) was limited by the maximal beam height available at beamline BL-14B. Visibilities of the interference pattern were measured at 15 points and ranged from 60% to 91% (average 79%, standard deviation 8%). This value is comparable with that achieved by smaller interferometers and is sufficient for phase-contrast X-ray imaging.

Fringes appearing in Fig. 2 are caused by the deformation and/or lattice strain of the interferometer. When such a built-in fringe pattern appears, it is difficult to understand the image contrast obtained in the interference pattern. However, using phase-shifting X-ray interferometry, the built-in fringe pattern can be removed as a background phase map, and a pure phase map, like that shown in Fig. 3(*a*), can be obtained.

A phase map corresponds to a projection of the refractive index. Therefore, when the thickness of a sample is constant and structural variation along the beam axis is negligible, a phase map approximates the distribution of the refractive index. A slice of a pathological specimen of human HCC was cut so as to satisfy such a requirement. Consequently, portions of the HCC lesion, surrounding necrosis, hemorrhagic necrosis, normal liver tissue and the vessel were revealed in Fig. 3(*a*). According to our previous observation with phase-contrast X-ray computed tomography, the fibrous capsule surrounding a cancer should cause contrast (Takeda *et al.*, 1998; Takeda, Momose, Yu *et al.*, 2000;

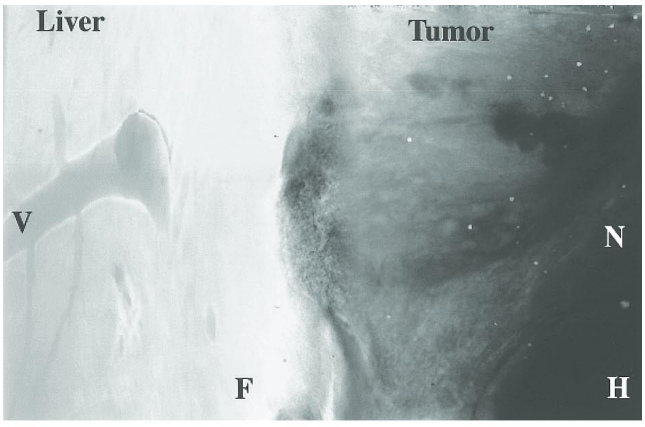

(*a*)

(*b*)

Figure 3
(*a*) Phase map and (*b*) pathological picture of a sliced human hepatocellular carcinoma. The scale bar is 2 mm. In the phase map the carcinoma lesion is shown as a granular grey structure ('Tumor') with a black irregular rod (focal hemorrhagic necrosis). Large hemorrhagic necrosis (H) and non-hemorrhagic necrosis (N) are shown as black and dark grey, respectively. The fibrotic capsule (F) between the normal liver and HCC lesions is depicted in white. A vessel (V) in normal liver is shown as a ductal structure with grey contrast.

Takeda, Momose, Hirano *et al.*, 2000). However, the corresponding contrast did not appear clearly in Fig. 3(*a*). It is speculated that the fibrous capsule was not parallel to the X-ray beam axis and the contrast was degraded. A vessel in normal liver was clearly depicted as grey contrast because of the significant difference in refractive index between the water in the vessel and normal liver. Revealed structures in the phase map were similar to those of the pathological picture.

4. Conclusions and future plans

A large monolithic X-ray interferometer has been fabricated, and its visibility was sufficient for phase-contrast X-ray imaging. Phase-contrast X-ray computed-tomographic images of large samples and phase maps of living objects have been measured.

In order to image objects of more than 100 mm for clinical application, the monolithic X-ray interferometer must be fabricated from a highly perfect single-crystal silicon ingot of diameter 300 mm. However, such ingots are not currently available. Alternatively, a separate-type interferometer (Momose *et al.*, 1997; Yoneyama *et al.*, 1999), a smaller version of which has already been constructed (Becker & Bonse, 1974), is now being developed to create a larger field of view.

This research was partially supported by the Special Coordination Funds for Promoting Science and Technology from the Science and Technology Agency of the Japanese Government. Experiments were performed under proposal number 97G164 and 99S002 approved by the High Energy Accelerator Research Organization.

References

Becker, P. & Bonse, U. (1974). *J. Appl. Cryst.* **7**, 593–598.
Beckmann, F., Bonse, U. & Biermann, T. (1999). *Proc. SPIE*, **3772**, 179–187.
Beckmann, F., Bonse, U., Busck, F. & Gunnewig, O. (1997). *J. Comput. Assist. Tomogr.* **21**, 539–553.
Bonse, U. & Hart, M. (1965). *Appl. Phys. Lett.* **6**, 155–156.
Momose, A. (1995). *Nucl. Instrum. Methods*, A**352**, 622–628.
Momose, A. & Fukuda, J. (1995). *Med. Phy.* **22**, 375–379.
Momose, A., Takeda, T., Itai, Y. & Hirano, K. (1996*a*). *Nature Med.* **2**, 473–475.
Momose, A., Takeda, T., Itai, Y. & Hirano, K. (1996*b*). *Proc. SPIE*, **2708**, 674–684.
Momose, A., Takeda, T., Itai, Y. & Hirano, K. (1998). *X-ray Microscopy and Spectromicroscopy*, edited by J. Thieme, G. Schmahl, E. Umbach & D. Rudolph, pp. II/207–212. Heidelberg: Springer-Verlag.
Momose, A., Takeda, T., Itai, Y., Tu, J. & Hirano, K. (1999). *Proc. SPIE*, **3659**, 365–374.
Momose, A., Takeda, T., Itai, Y., Yoneyama, A. & Hirano, K. (1998). *J. Synchrotron Rad.* **5**, 309–314.
Momose, A., Yoneyama, A. & Hirano, K. (1997). *J. Synchrotron Rad.* **4**, 311–312.
Takeda, T., Momose, A., Hirano, K., Haraoka, S., Watanabe, T. & Itai, Y. (2000). *Radiology*, **214**, 298–301.
Takeda, T., Momose, A., Itai, Y., Wu, J. & Hirano, K. (1995). *Acad. Radiol.* **2**, 799–803.
Takeda, T., Momose, A., Ueno, E. & Itai, Y. (1998). *J. Synchrotron Rad.* **5**, 1133–1135.
Takeda, T., Momose, A., Yu, Q., Yuasa, T., Dilmanian, F. A., Akatsuka, T. & Itai. Y. (2000). *Cell. Mol. Biol.* In the press.
Yoneyama, A., Momose, A., Seya, E., Takeda, T. & Itai, Y. (1999). *Rev. Sci. Instrum.* **70**, 4582–4586.